The Astronomical Journal, 147:149 (13pp), 2014 June doi:10.1088/0004-6256/147/6/149

STUDY OF ECLIPSING BINARY AND MULTIPLE SYSTEMS IN OB ASSOCIATIONS. II. THE CYGNUS OB REGION: V443 Cyg, V456 Cyg, AND V2107 Cyg

V. Bakış[1], H. Hensberge[2], S. Bilir[3], H. Bakış[1], F. Yılmaz[4], E. Kiran[5], O. Demircan[6], M. Zejda[7], and Z. Mikulášek[7]
[1] Faculty of Science, Department of Space Sciences and Technologies, Akdeniz University, Antalya, Turkey
[2] Royal Observatory of Belgium, Ringlaan 3, B-1180 Brussels, Belgium
[3] Science Faculty, Department of Astronomy and Space Sciences, İstanbul University, 34119 University-İstanbul, Turkey
[4] Physics Department, Çanakkale Onsekiz Mart University, Terzioğlu Campus, TR-17020 Çanakkale, Turkey
[5] Faculty of Science, Department of Astronomy and Space Sciences, Ege University, Izmir, Turkey
[6] Department of Space Sciences and Technologies, Çanakkale Onsekiz Mart University, Terzioğlu Campus, TR-17020 Çanakkale, Turkey
[7] Department of Theoretical Physics and Astrophysics, Masaryk University, Brno, Czech Republic
Received 2013 April 24; accepted 2014 March 6; published 2014 May 8

ABSTRACT

Three presumably young eclipsing binary systems in the direction of the Cygnus OB1, OB3, and OB9 associations are studied. Component spectra are reconstructed and their orbits are determined using light curves and spectra disentangling techniques. V443 Cyg and V456 Cyg have circular orbits while the light curve of V2107 Cyg imposes a slightly eccentric orbit ($e = 0.045 \pm 0.03$). V443 Cyg harbors F-type stars, not young early-A stars as previously suggested in the literature based solely on photometry. It appears to be situated in the foreground (distance 0.6 ± 0.2 kpc) of the young stellar populations in Cygnus. V456 Cyg, at a distance of 0.50 ± 0.03 kpc, consists of a slightly metal-weak A-type star and an early-F star. The age of both systems, on or very near to the main sequence, remains uncertain by an order of magnitude. V2107 Cyg is a more massive system (8.9 ± 2 and $4.5 \pm 1.2\,M_{\odot}$) at 1.5 ± 0.5 kpc and, also kinematically, a strong candidate-member of Cyg OB1. The more massive component is slightly evolved and appears to undergo non-radial βCep-type pulsations. The Doppler signal of the secondary is barely detectable. A more extensive, asteroseismological study is necessary to fix masses more precisely. Nevertheless, the position of the primary in the H-R diagram confines the age reasonably well to 20 ± 5 Myr, indicating that for Cyg OB1 has a similar extent of star formation history as that established for Cyg OB2.

Key words: binaries: eclipsing – stars: distances – stars: fundamental parameters

Online-only material: color figures, supplemental data

1. INTRODUCTION

The star-forming regions in the constellation Cygnus are among the most active regions of star birth in our Galaxy. An overview of these regions is presented in Reipurth & Schneider (2008). These authors emphasized the confusion of regions as near as hundreds of parsecs with regions at 1–2 kpc and even well beyond due to the fact that when observing in the direction of Cygnus, one is looking down a spiral arm. Kinematical distances suffer from the fact that the radial velocity (RV) gradient up to 4 kpc is smaller than the typical velocity dispersion of interstellar gas. As a consequence, even the need for the nine classical subgroups OB1 to OB9 in Cygnus is still debated, with some researchers suggesting, for example, that OB1, OB8, and OB9 might actually form a single subgroup (Mel'nik & Efremov 1995). Hence, distances derived from young eclipsing binary systems are of value to localize the star-forming regions and stellar associations.

A major study of binary stars in Cygnus has focused on Cyg OB2, the most famous, and probably also the youngest, subgroup. The Cyg OB2 RV survey now encompasses 25 massive binaries (Kobulnicky et al. 2012; Kiminki & Kobulnicky 2012). Another very recent study (Mahy et al. 2013) focuses on bright O-type stars. Two hundred seventy-four spectra taken over three years reveal four spectroscopic binaries (three in Cyg OB1 and one in Cyg OB9; none in either Cyg OB3 or Cyg OB8). Earlier studies discuss binary stars in open clusters superposed on Cyg OB1. Zakirov (1999) presents three eclipsing binaries with early-B primary components which are plausible members of the open cluster IC 4996, but *UBVR* photometry without orbital-phase resolved spectroscopy did not lead to precise fundamental parameters. Boeche et al. (2004) detect 9 binaries out of 16 stars in the direction of NGC 6913, including 7 binary stars (1 eclipsing) among the 12 presumed cluster members. They adopt a distance of 1.6 kpc to NGC 6913, but emphasize (their Figure 2) that the cluster distance cannot be well constrained. Very recently, 60 eclipsing systems in the field of the Cygnus OB7 star-forming region were identified by Wolk et al. (2013) from *JHK* photometry in 100 nights spanning 1.5 yr. A minority of them (23) are detached systems with orbital periods between $0\overset{d}{.}4$ and just over 13 days, and a majority (37) show continuous flux variations with periods ranging from $0\overset{d}{.}2$ to 3 days. Most of the latter are thought to be W UMa contact binaries. These stars have *J*-band magnitudes from 12.5 to 17.3, and are identified as diskless field stars. W UMa-type contact binaries are not observed in clusters younger than about 1 Gyr. We did not find any literature on later-type binary stars unequivocally identified as members of the young associations.

The stars discussed in this paper are situated in the OB1–OB3–OB9 region. Two of them are suspected to be pre-main-sequence systems with A-type components based on photometric studies (Zakirov & Eshankulova 2005, 2006). They suggest the stars are connected to Cyg OB9 (V443 Cyg) and to a group of OB stars in the direction of Cyg OB1 (V456 Cyg). Nelson (2011) points out the lack of spectroscopic knowledge for V456 Cyg and leaves open the question of whether the primary component of this system is an early-A or a late-A star. The third object, V2107 Cyg (HD 191473), is an early-B system

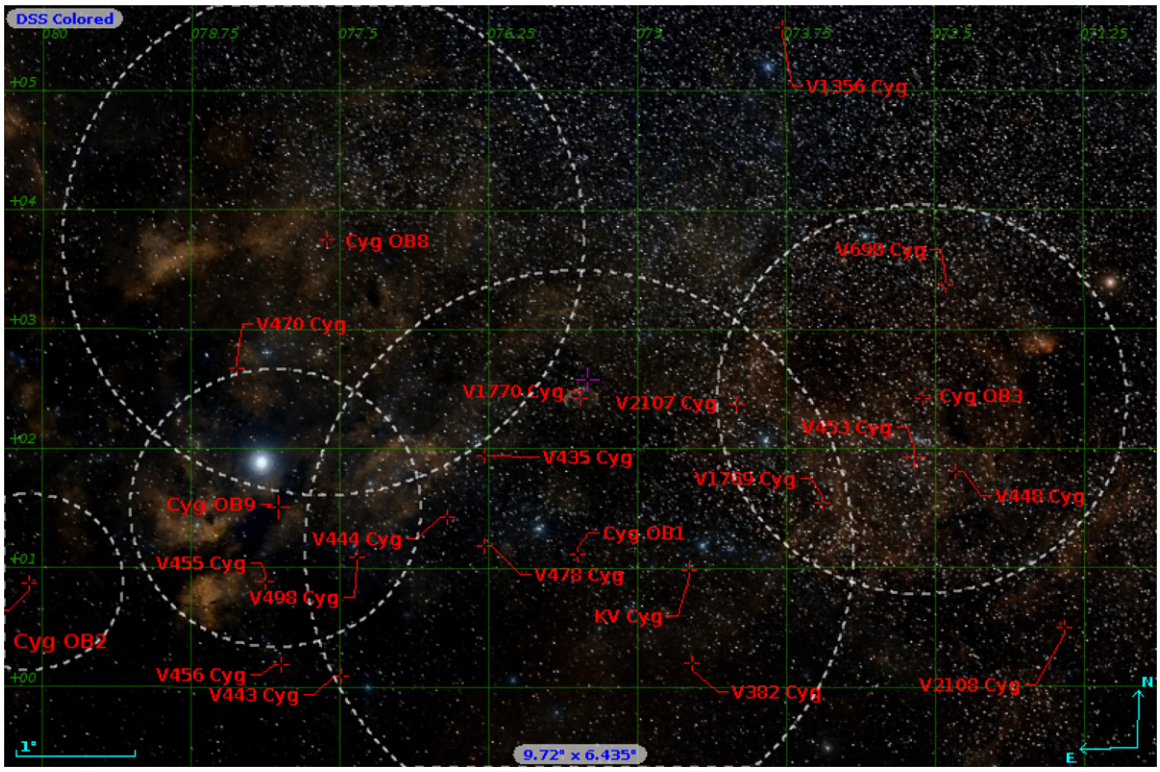

Figure 1. Region of OB1, 2, 3, 8, 9 stellar associations in Cygnus according to partitions of Blaha & Humphreys (1989).

at the end of or slightly off the main sequence with a primary component of luminosity class III to IV (B0.5 III, Roman 1951; B0 IV, Morgan et al. 1955; B1 III, Walborn 1971), and thus a particularly interesting age calibrator. Their position in the Cygnus region, relative to the stellar subgroups, is shown in Figure 1.

In this paper, we summarize the characteristics of the observations and the analysis methodology applied (Sections 2 and 3). Thereafter, each of the three binary systems is discussed in turn (Sections 4–6) and the general conclusions are presented in Section 7.

2. OBSERVATIONS

For each object, spectra at 11 to 15 orbital phases were obtained, and the light curve was covered completely in thousands of CCD frames obtained from 2009 to 2011 using various broadband filters. The log of the observations is given in Tables 1 (spectroscopy) and 2 (photometry).

2.1. Spectroscopy

The spectra of V443 Cyg and V456 Cyg were taken with the Faint Object Spectrograph and Camera (TFOSC) installed at the Cassegrain focus of the 1.5 m RTT telescope (RTT150) of TÜBİTAK National Observatory (TUG), Turkey ($\sim 36^\circ 49^m$ N, $30^\circ 20^m$ E, altitude 2500 m). The highest resolution mode was used ($R(\lambda/\delta\lambda) \sim 5100$). The list of grisms and the resulting resolutions can be found in the instrument's manual.[8] The CCD chip has 2048×2048 pixels of 15×15 μm each. The wavelength range from 3300 to 9000 Å is covered completely in 11 échelle orders. All spectra were obtained in three observing sessions (2011 September, 2011 August, 2011 October).

The spectroscopic observations of V2107 Cyg were performed at two sites. The Coudé/Échelle Spectrograph (CES) at the RTT150 telescope of TUG gives spectra with a resolving power of $R \sim 40{,}000$ and covers the wavelength range from 3960 to 8770 Å in 68 spectral orders on an SAO RAS A 1024×1024 nitrogen-cooled CCD camera (see Bikmaev et al. 2005 for technical details). The échelle spectrograph HERMES (Raskin et al. 2011) at the 1.2 m Mercator telescope[9] was used in high-resolution mode ($R \approx 80{,}000$). It covers the wavelength range from 3700 to 9000 Å in 55 échelle orders, with small gaps between the extreme reddest orders. Five to six consecutive exposures of 600 s keep the Doppler shifts during a single exposure below 1 (2) km s^{-1} for the primary (secondary), respectively, and provide a total signal-to-noise ratio near 150 over a broad range. The data reduction pipeline of the spectrograph was used with the calibration frames available in standard operation mode, complemented by personally written programs in the ESOMIDAS package for continuum definition and removal of weaker cosmic rays by intercomparison of the subsequent exposures.

2.2. Photometry

Photometry was performed at the Ulupınar Observatory of Çanakkale Onsekiz Mart University ($\sim 40^\circ 06^m$ N, $26^\circ 30^m$ E, altitude 410 m). Schmidt–Cassegrain-type telescopes and Alta back-illuminated CCD detectors (Apogee ^{TM}) were used. Bias and dark frame subtraction and flat field division was done using the IRAF platform. The C-MUNIPACK[10] software was used to perform aperture photometry with aperture sizes three times the nightly FWHM values of the stellar images. Initially, several

[8] http://www.tug.tubitak.gov.tr/rtt150_tfosc.php

[9] The Mercator Telescope is operated on the island of La Palma by the Flemish Community at the Spanish Observatorio del Roque de los Muchachos of the Instituto de Astrofsica de Canarias.

[10] http://c-munipack.sourceforge.net/

Table 1
Log of Spectroscopic Observations for Program Stars

No.	HJD (−2,400,000)	t_{exp} (s)	S/N	ϕ (ϕ)	Z	HJD (−2,400,000)	t_{exp} (s)	S/N	ϕ (ϕ)	Z	HJD (−2,400,000)	t_{exp} (s)	S/N	ϕ (ϕ)	Z
	V443 CYG					**V456 CYG**					**V2107 CYG**				
1	55455.3990	1200	50	0.477	1.19	55455.3562	1200	155	0.291	1.07	55700.6345	3000	150	0.008	1.18
2	55455.4181	1200	50	0.489	1.27	55455.3758	1200	130	0.313	1.11	55790.6158	3600	150	0.009	1.30
3	55455.4571	1200	50	0.512	1.51	55455.4330	1200	120	0.377	1.34	55743.5015	3000	150	0.013	1.21
4	55455.4751	1200	50	0.523	1.67	55455.4911	1200	105	0.443	1.84	55161.2543	3600	40	0.120	1.56
5	55456.3061	1200	45	0.023	1.01	55456.2268	1200	130	0.268	1.04	55161.2978	3600	40	0.130	2.11
6	55456.4785	1200	30	0.127	1.74	55456.3346	1200	100	0.389	1.04	55162.1473	3600	65	0.328	1.07
7	55456.4960	1200	50	0.137	1.96	55456.5170	1200	110	0.594	2.30	55162.1908	3600	50	0.338	1.20
8	55457.3371	1200	40	0.643	1.05	55456.5320	1200	110	0.611	2.65	55775.6135	3000	150	0.507	1.12
9	55457.3584	1200	50	0.656	1.09	55457.3141	1200	80	0.488	1.02	55163.1388	3600	60	0.560	1.06
10	55457.4734	1200	50	0.725	1.71	55457.4390	1200	90	0.628	1.41	55163.1822	3600	60	0.570	1.18
11	55457.5399	1200	50	0.765	3.04	55457.5106	1200	95	0.709	2.23	55163.2256	3600	60	0.580	1.39
12						55795.4336	1800	150	0.888	1.09	55164.1764	3600	50	0.802	1.17
13											55164.2199	3600	55	0.812	1.37
14											55164.2633	3600	55	0.822	1.74
15											55160.2510	3600	50	0.886	1.51

Note. Signal-to-noise (S/N) ratio refers to the continuum near 6500 Å.

Table 2
Log of Photometric Observations for Program Stars

Star Mag., Colors	Comparison/Check Star Mag.	Telescope(s) / Detector(s)	Filter(s)	Number of Data
V443 Cyg	GSC 3152 1079/GSC 3152 567	122-cm / Alta U42	*B*	409
$V = 12.31$	13.47 / 12.36		*V*	460
$B - V = 0.51$			*R*	531
$U - B = 0.05$				
V456 Cyg	GSC 3152 491/GSC 3152 439	40-cm / Alta U47	*U*	1174
$V = 10.80$	11.12 / 10.53		*B*	1200
$B - V = 0.31$	0.073 / 0.3		*V*	1207
$U - B = 0.11$			*R*	1213
			I	1204
V2107 Cyg	GSC 2683 1295/GSC 2683 191	40-cm–30-cm / Alta U47, U42–U47	*U*	5752
$V = 8.63$	11.19 / 9.51		*B*	5885
$B - V = 0.10$	0.42 / 0.41		*V*	6307
$U - B = -0.60$			*R*	7242

comparison and check stars were measured and those giving the lowest standard deviations in their differential magnitudes were selected for final differential photometry.

3. METHODOLOGY

Orbital periods are taken from the literature (V443 Cyg and V456 Cyg) or determined by combining our data with published measurements (V2107 Cyg) in order to gain precision by exploiting much longer time baselines than covered by our own data alone. As a preliminary step, RVs were measured on the spectra for a few individual lines as far as line blending and component intensity allow. Together with published RVs, they were used with the purpose of obtaining initial orbital parameters for the Fourier spectra disentangling codes *korel* (Hadrava 1995) and *fdbinary* (Ilijić 2003)[11]. These codes solve for the pure Keplerian orbit and deliver component spectra that are used to determine spectral types and, in particular, the temperature of the primary component. Thereafter, the light curves of the eclipsing systems are modeled, using the PHOEBE LC package (Prša & Zwitter 2005) which uses the Wilson–Devinney code (Wilson & Devinney 1971), inclusive the stellar atmosphere model (Kurucz 1993) and a detailed reflection treatment (Wilson 1990). Circular orbits represent well the data for V443 Cyg and V456 Cyg. The orbit of V2107 Cyg is very slightly eccentric. The photometry puts a lower limit to $e \cos \omega$ and the spectroscopic solution must be tuned for consistency in the time of periastron passage (Section 6). The mass ratio for the three systems was fixed to the value obtained from the spectroscopy.

The light curve models used albedos $A_{1,2}$ and gravity darkening coefficients $g_{1,2}$ set to the generally adopted values (Rucinski 1973; Lucy 1967). Two-dimensional logarithmic limb-darkening coefficients were interpolated from the values given by van Hamme (1993). The temperature of the primary components were set to the spectroscopically estimated values. Semi-detached and detached configurations were tested. All three systems turn out to be well inside their Roche lobes.

4. V443 CYG

The orbital period of V443 Cyg is $1^d.66220545$ (Zakirov & Eshankulova, 2005). The spectra disentangling codes converge to solutions with mass ratio close to unity (Table 3), both in the H_α and the λ4400 regions. We used the jackknife method (see, e.g., Bissell & Ferguson 1975) to estimate the uncertainties and

[11] See also http://sail.zpf.fer.hr/fdbinary.

Table 3
Orbital Solutions of V2107 Cyg based on the M57 data

Parameter	M57	LS71	ecc	cir	jack
K (km s^{-1})	106.5	106.8	107.3 ± 1.6	104.6	106.0 ± 4.0
e	0.045	0.070	0.073 ± 0.015	0	0.06 ± 0.03
ω(deg)	134	122	121 ± 14		115 ± 17
$T_p - 2\,435\,400$	30.78	29.158	30.60 ± 0.01		30.53 ± 0.20
V_{sys} (km s^{-1})	−3.7	−3.8	−3.8	−3.9	
$f(M)$ ($M_\odot$)	0.53	0.54	0.54	0.51	0.53
$\sigma(O-C)$ (km s^{-1})	4.8	5.0	4.3	6.5	

Notes. LS71 refers to Lucy & Sweeney (1971). The last three columns contain our computations (least-squares eccentric orbit, least-squares circular orbit, jackknife bias-corrected orbit).

Table 4
Spectroscopic Orbital Parameters of Program Stars

Parameter	V443 Cyg	V456 Cyg	V2107 Cyg	
			Sol.1	Sol.2
P (days)	1.66220545(43)	0.89119559(17)	4.2845923(25)	
T_0 (HJD− 2,450,000)	5456.2677(0.0025)	5455.0966(0.0016)	5259.3024(0.0004)	
K_1 (km s^{-1})	117.4 (6.2)	152.1 (1.7)	104 (1.5)	
K_2 (km s^{-1})	120.2 (4.2)	179.4 (1.7)	187 (5)	207(20)
e [fixed]	0.0	0.0	<0.03	
V_γ (km s^{-1})	−19.7 (0.7)	−4.2 (1.0)	-6.3 (0.2)	
$q(M_2/M_1)$	0.977(0.067)	0.848(0.018)	0.56(0.02)	0.50(0.06)

Note. The numbers between brackets behind the value of the period are the uncertainties in the last digits of P.

bias in the parameters, leaving out one spectrum at a time. It reveals that the size and orbital phase distribution of the present set of spectra is near the lower limit required for a robust orbital solution. For example, in the λ4400 region including Hγ and Mg II λ4481, we have 9 instead of 11 useful spectra (the 2 additional ones being too noisy in the blue due to high airmass) and the orbit solution is instable in the sense that leaving out one more spectrum may change the mass ratio by 15%. Thus, the precision of the orbit solution relies on the redder part of the spectrum. A significant gain in precision could be obtained by doubling the data set. For example, allowing for (unexplained) subpixel shifts in two spectra that are least consistent with the whole set reduces the uncertainties by a factor of two. This gives an impression of the sensitivity of the present solution to data reduction and/or calibration issues (or to the assumption of the Doppler shifts reflecting a purely Keplerian orbit). The orbit derived from the spectra disentangling is given in Table 4.

The component spectra obtained in the two mentioned wavelength regions (Figure 2) indicate F-type components, in contrast to the expectation of Zakirov & Eshankulova (2005) whose photometric analysis pointed to young A-type stars. The brightest component of V443 Cyg is similar to HD 128167, while the faintest component is similar to HD 38393, but apparently H_α is partly filled-in with emission (Figure 2). HD 128167 (σ Boo) is an F2V star. Most studies agreed on $T_{\rm eff} \approx 6700$ K, $\log g \approx 4.3$ and [Fe/H] ≈ -0.4 dex (Edvardsson et al. 1993; Gratton et al. 1996; Cunha et al. 2000; Cenarro et al. 2007). In view of its spectral type F2/3 V, the effective temperature of the primary is fixed to 6700 K in the light-curve analysis. HD 38393 is classified F6.5 V (Gray et al. 2006). Most studies agree on $T_{\rm eff} \approx 6350$ K, $\log g \approx 4.3$ and [Fe/H] ≈ -0.1 dex (Edvardsson et al. 1993; Gray et al. 2006; Cenarro et al. 2007). Hence, V443 Cyg contains an early-F and a mid-/late-F star.

Figure 7 shows the best-fitting LC models and Table 5 the associated parameters. Table 6 lists the characteristics of

Table 5
Results from the Simultaneous Solution of LCs of Program Stars in Several Filters

Parameter Adjusted	V443 Cyg	V456 Cyg	V2107 Cyg
$T_{\rm eff2}(K)$	6200(11)	6755(10)	15200(100)
$L_1/L_{1+2}(U)$	0.700(0.010)	0.653(0.010)	...
$L_1/L_{1+2}(B)$	0.694(0.007)	0.693(0.007)	0.942(0.001)
$L_1/L_{1+2}(V)$	0.665(0.005)	0.672(0.002)	0.938(0.001)
$L_1/L_{1+2}(R)$	0.658(0.004)	0.639(0.005)	0.943(0.001)
$L_1/L_{1+2}(I)$	...	0.624(0.002)	...
$L_1/L_{1+2}(Hp)$	...	...	0.938(0.002)
Ω_1	6.78(0.04)	4.388(0.010)	4.17(0.01)
Ω_2	8.18(0.04)	4.500(0.006)	7.32(0.01)
$\Omega_{\rm cr}$	3.73	3.49	2.99
r_1(mean)	0.172(0.020)	0.285(0.008)	0.280(0.003)
r_2(mean)	0.140(0.030)	0.250(0.005)	0.092(0.005)
i(°)	89.9(0.5)	82.9(0.4)	86.2(0.5)
e	0.0	0.0	0.045(0.03)
w(°)	...	...	102 (2)
Fixed:			
P (days)	1.66220545	0.89119559	4.2845923
T_0	2,455,454.6041	2,455,455.0958	2,455,259.3024
$T_{\rm eff1}(K)$	6700	7750	22500
$q(M_2/M_1)$	0.98	0.85	0.50
$A_1 = A_2$		1.0	
$g_1 = g_2$		1.0	
$F_1 = F_2$		1.0	

Notes. Adjusted and fixed parameters are presented in separate panels of the table. Uncertainties of adjusted parameters, as suggested by the Wilson–Devinney code, are given in brackets.

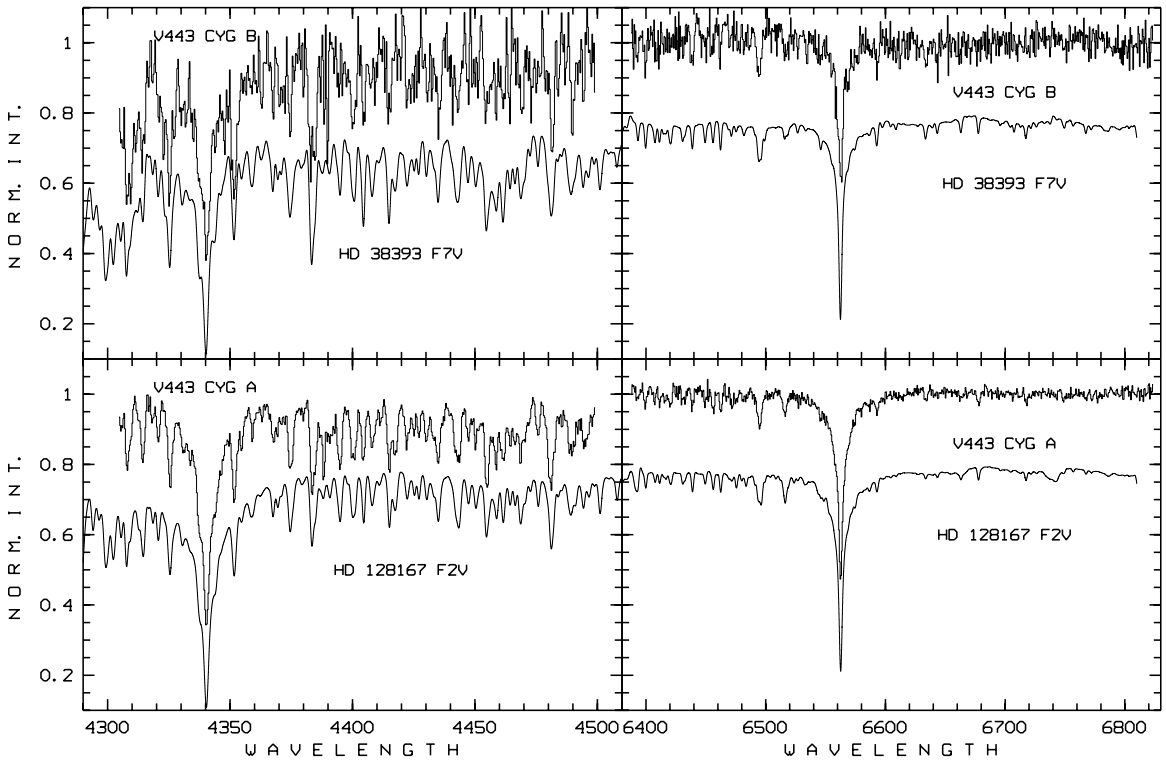

Figure 2. Reconstructed component spectra of V443 Cyg, compared to spectra of bright stars in the ESO UVES POP library degraded to the resolution of the TFOSC spectra of V443 Cyg.

(Supplemental data of this figure are available in the online journal.)

Table 6
Close Binary Stellar Parameters of the Program Stars

Parameter	V443 Cyg		V456 Cyg		V2107 Cyg	
	Primary	Secondary	Primary	Secondary	Primary	Secondary
Sp	F2/3V	F8V	A2hA7mA4V	F3V	B1III	...
M ($M_\odot$)	1.2(0.2)	1.1(0.3)	1.86(0.06)	1.58(0.05)	8.9(2.0)	4.5(1.3)
R ($R_\odot$)	1.3(0.2)	1.1(0.2)	1.68(0.02)	1.47(0.02)	7.4(0.6)	2.4(0.3)
a ($R_\odot$)	9.40(0.33)		5.88(0.06)		26.4(1.9)	
P (days)	1.66220545(43)		0.89119559(17)		4.2845923(25)	
i (°)	89.9(0.5)		82.9(0.4)		86.2(0.5)	
q (M_2/M_1)	0.98(0.09)		0.85(0.02)		0.50(0.06)	
R_L ($R_\odot$)	3.54		2.15		8.57	
e	0.0		0.0		<0.03	
log g (cgs)	4.25(0.23)	4.42(0.26)	4.258(0.027)	4.302(0.027)	3.65(0.17)	4.3(0.2)
V (mag)	12.31(0.03)		10.80(0.03)		8.63(0.02)	
$B-V$ (mag)	0.51(0.09)		0.31(0.02)		0.10(0.05)	
$E(B-V)$ (mag)	0.13(0.15)		0.11(0.05)		0.335(0.045)	
A_v (mag)	0.42(0.15)		0.35(0.08)		1.04(0.14)	
$(B-V)_0$ (mag)	0.38(0.06)		0.20(0.02)		−0.23(0.05)	
$T_{\rm eff}$ (K)	6700(350)	6200(550)	7750(100)	6755(400)	22500(1500)	15200(1600)
log L ($L_\odot$)	0.52(0.27)	0.20(0.21)	0.96(0.05)	0.61(0.06)	4.10(0.18)	2.5(0.5)
$M_{\rm bol}$ (mag)	3.46(0.67)	4.25(0.53)	2.35(0.11)	3.23(0.14)	–5.5(0.5)	–1.4(1.2)
M_v (mag)	3.44(0.65)	4.27(0.53)	2.32(0.12)	3.21(0.14)	–3.4(0.6)	–0.1(1.2)
BC (mag)	0.02(0.02)	–0.02(0.05)	0.03(0.01)	0.02(0.01)	–2.2(0.2)	–1.3(0.2)
$K_{1,2}$ (km s^{-1})	117.4(6.2)	120.2(4.2)	152.1(1.7)	179.4(1.7)	104(1.5)	207(20)
V_γ (km s^{-1})	−19.7(0.7)		–2.7(1.0)		–6.3(0.2)	
$V_{\rm synch}$ (km s^{-1})	41(7)	33(6)	95(1)	83(1)	87(7)	29(4)
$V_{\rm rot}$ (km s^{-1})	...	...	100(10)	...	84(4)	...
d (pc)	600(200)		500(30)		1500(500)	
$\mu_\alpha cos\delta$, μ_δ (mas yr^{-1})	–11.1(2.2), –15.8(2.2)		5.6(1.2), 1.3(1.1)		–4.8(1.3), –6.5(1.3)	
U (km s^{-1})	48.98(22.39)		–10.66(2.73)		49.76(19.06)	
V (km s^{-1})	–31.05(5.02)		–0.46(1.14)		–20.79(5.46)	
W (km s^{-1})	–0.57(6.22)		–9.02(2.84)		3.14(8.70)	

Note. Uncertainties of parameters are given in brackets.

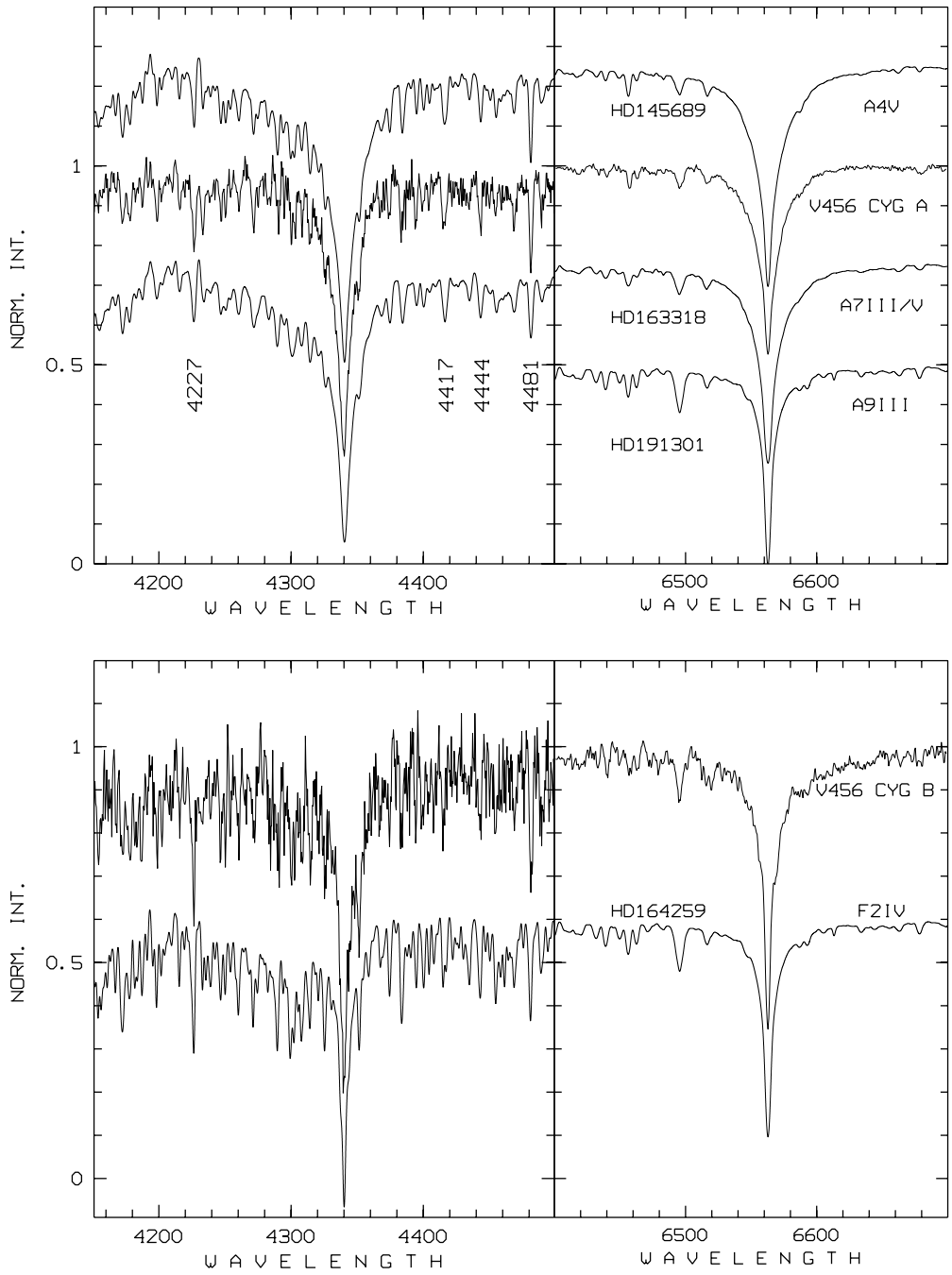

Figure 3. Upper: parts of the disentangled spectrum of V456 Cyg A compared to UVES POP spectra of A-type stars degraded to the resolution of the TFOSC instrument. The UVES POP spectra were normalized by tracing a linear approximation to the continuum in each of the regions. Velocity shifts were applied to all spectra to ease comparison of spectral lines. Lower: parts of the disentangled spectrum of V456 Cyg B compared to an early-F star in the UVES POP library.

(Supplemental data of this figure are available in the online journal.)

the components and the orbit, as derived from the combined spectroscopic-photometric analysis. The masses and radii are, within the substantial uncertainties, compatible with the spectral types. The system is significantly less massive than the 3.2 + 2.5 $M_{\odot}$ mentioned by Zakirov & Eshankulova (2005), and has a mass ratio much nearer to unity. Component masses are of the order of 1.1 to 1.2 $M_{\odot}$. The difference in spectral type and temperature is better compatible with a mass ratio around 0.9 (which is within the error bars of the present analysis) than with the best nominal value $M_2/M_1 = 0.98$ (see Figure 8). For such a light system still near the zero-age main sequence, the exact age is largely uncertain. Isochrones derived from the tracks of Bertelli et al. (2009), where initial rotation velocity for tracks and isochrones is not taken into account, show that the system might be either as young as 2×10^7 yr or more than one Gy old. The system is at a distance of 0.6 ± 0.2 kpc.

5. V456 CYG

In accordance with Nelson (2011), we used an orbital period of $0^{\rm d}.89119559$. Zakirov & Eshankulova (2006) suggested a parabolic trend in the $O-C$ diagram of V456 Cyg. However, this assumption leads to less consistency between our light and RV data that were obtained at different epochs. Moreover,

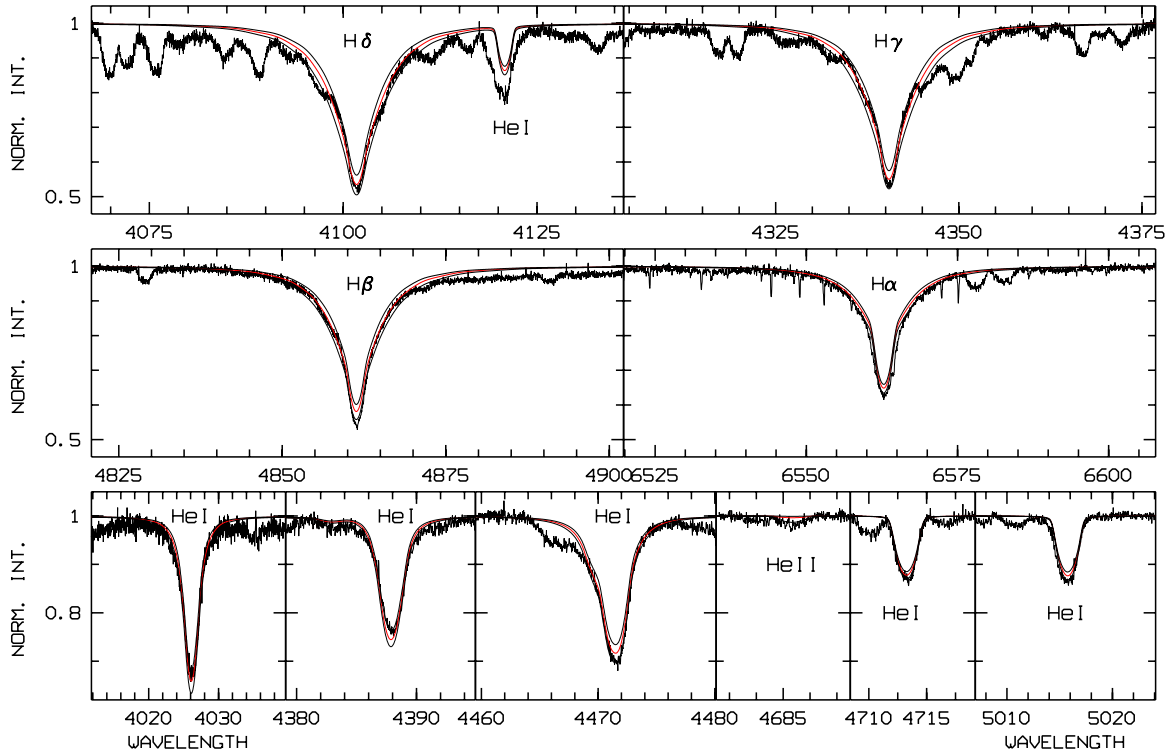

Figure 4. Hydrogen and helium lines in total eclipse of V2107 Cyg (pure spectrum of the primary) compared to models for $\log g = 3.6$ cgs (see Table 6) and effective temperatures of 20,000 (black line), 22,000 (red line), and 24,000 K (black line). The red line is the fit for the intermediate temperature. Deeper absorption in the models corresponds to lower temperature, except for the He II line. Notice that He I λ4121 is heavily blended by metal lines, while the red wing of H_β is affected by a diffuse interstellar band.

(A color version and supplemental data of this figure are available in the online journal.)

we notice that the more recent orbital period published in Hoffman et al. (2008), $P_{\rm NSVS} = 0\overset{d}{.}61634$, based on the NSVS photometry (Wozniak et al. 2004), is an alias of the true period, $P_{\rm NSVS}^{-1} - P_{\rm true}^{-1} = 0.5004$. This is in disagreement with the extensive list of eclipse timings in the literature and the same is true for several other stars in that paper.

The RVs given by Nelson (2011), shifted by −4.6 km s^{-1}, were used together with ours to determine the initial parameters for the spectra disentangling codes. This shift was determined by comparing the linear relation between the RVs of both components for both data sets, with the gradient giving the mass ratio q (identical for both sets) and the zero-point defined by $(1+q)V_\gamma$. While not stated explicitly in his paper, we suspect that the velocities of Nelson, determined via the use of templates, are relative to the systemic velocity of the system rather than on an absolute velocity scale. The applied shift is estimated to be uncertain by 1.5 km s^{-1}.

The orbit derived from the spectra disentangling is given in Table 4. When analyzed separately, the Nelson RVs give 5% lower velocity amplitudes. Therefore, the formal uncertainties (1%) on K_1 and K_2 should be interpreted with caution. Uncertainties of 2.5% on the masses may be more realistic.

The reconstructed component spectra of V456 Cyg (Figure 3) definitely rule out Nelson's (2011) Model 1. The hydrogen lines of the primary are consistent with late-A type stars, with H_α suggesting A9 and Hγ rather than A7. The Balmer lines do not show the strongly stark broadened wings of early-A type stars, and the dynamical analysis does not leave space to consider higher luminosity. However, the ratios of λ4417 (Fe II and Ti II blend) and Ti II λ4444 to Mg II λ4481 suggest A4, and Ca I λ4227 and the Ca II K line (the latter of which is not disentangled, but when the secondary component is eclipsed) suggest A2. Thus, one is tempted to classify V456 Cyg A as a slightly metal-weak star, A2hA7mA4. Its rotation velocity is 100 ± 10 km s^{-1}. With the hydrogen lines being the most sensitive temperature parameter, the temperature of V456 Cyg A is fixed at 7750 ± 150 K for the light curve analysis.

The Mg II λ4481 line is stronger than Fe I λ4383, and the Mg II line does not show a greater weakening than the general metallic-line spectrum with respect to the hydrogen lines. As both of these criteria are contrary to what is seen in *most* λ Bootis stars (see, e.g., Gray 1988), the star very probably does not belong to this class. Whether the hydrogen lines are peculiar in a subtle way, as seen in λ Bootis-type stars, is not easily evaluated on the reconstructed spectrum.

The secondary component rotates significantly slower, but a precise estimate is hard at the TFOSC resolution. We set an upper limit of 50 km s^{-1} to $v \sin i$. The star shows a general resemblance to the degraded high-resolution UVES spectra of HD 164259, a F2IV star, although not perfectly. The noise level in the reconstructed spectrum of the fainter companion and the restricted resolution do not permit us to independently confirm a slightly low metallicity as seen in the primary.

The system certainly deserves a more detailed analysis at higher resolution. In conclusion, the reconstructed spectra show a system consisting of a late-A and early-F spectrum, with at least the primary being somewhat metal-weak.

Figure 7 shows the best-fitting LC models and Table 5 the associated parameters. Table 6 lists the characteristics of the components and the orbit, as derived from the combined spectroscopic-photometric analysis. Our solution is near to Nelson's (2011) Model 2, but different in some respects.

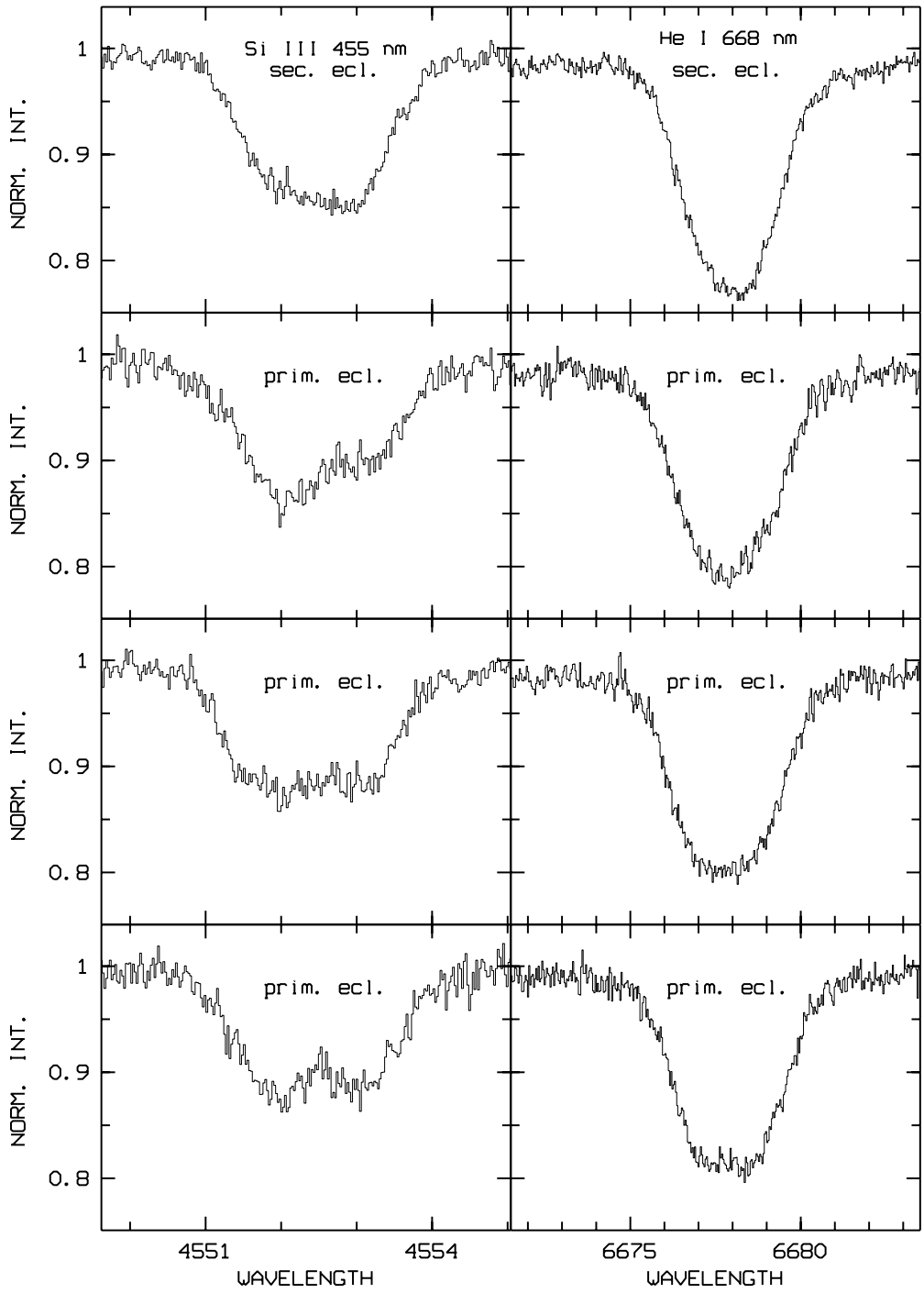

Figure 5. Line variability seen in two lines. The upper panel shows the spectrum of V2107 Cyg A (mid-secondary eclipse). The three lower panels show primary eclipse spectra taken during three different orbital cycles. In each case, five to six subsequent 10 minute exposures were added after small shifts to correct for the orbit.

Nelson's problem of disparate ages related to the radius of the less massive star and its $\log g$ being larger than for the primary does not survive in our solution ($1.68 + 1.47 R_{\odot}$; $\log g = 4.26 + 4.30$). We also find masses 8% higher (while agreeing on the mass ratio) and the luminosity of the primary exceeds Nelson's by 30%. The system is at a distance of 0.50 ± 0.03 kpc.

With the precision obtained for this system, a discussion of its position in the Hertzsprung–Russell diagram is interesting. The stars are slightly too cool and too small for their masses, unless a metallicity as high as $Z = 0.035$ is assumed. The least we can state is that the photosphere does not provide arguments for an enhanced metallicity. Therefore, it appears worthwhile to investigate the option that the system might be young, near to but still on its way to the main-sequence. A comparison with the tracks of Bertelli et al. (2009) shows an encouraging agreement (see Figure 8), although the less massive component is predicted further from the main-sequence than observed. In order to discern whether the system is arriving at the zero age main sequence (25 Myr), or older (315 Myr) with higher metallicity, more detailed spectroscopy is required. Any age between the quoted extremes is presently still an option.

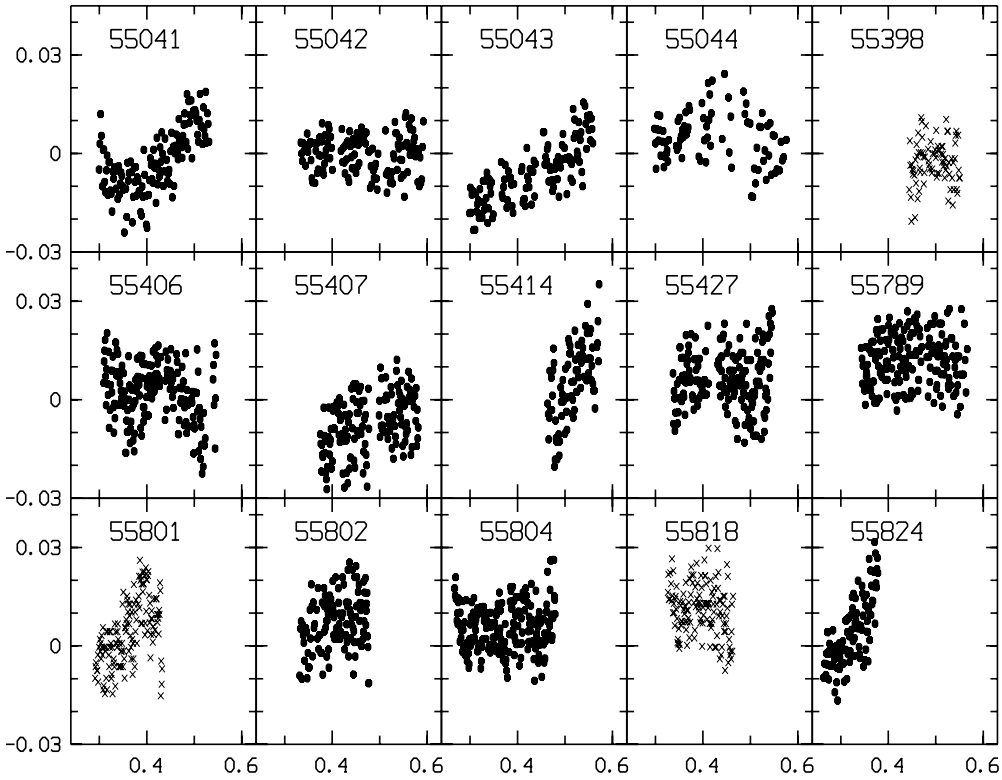

Figure 6. Photometric variability of residuals from the LC solution of V2107 Cyg. The number in each panel is Julian Day – 2,400,000.

6. V2107 CYG

Phasing our photometry together with the HIPPARCOS satellite photometry, the orbital period was fixed to $4\overset{d}{.}2846$. An earlier spectroscopic study (Mercier 1957, hereafter M57) suggested an orbit with small eccentricity ($e = 0.045$). In a paper rejecting low-eccentricity orbits for many systems Lucy & Sweeney (1971, hereafter LS71), confirmed that the orbit of V2107 Cyg is probably not circular ($p = 0.011$) and updated the orbital parameters, inclusive $e = 0.070$, after considering the bias in the determination of e (toward larger e for low e),. Therefore, a discussion of the reality of a non-circular orbit despite the four-day period is presented in Section 6.2.

Since the secondary star is occulted completely during six hours around phase 0.5, the spectrum of the hotter component (A) is observed directly. The spectrum of the secondary is not readily visible in any of the observed spectra, even after (scaled) subtraction of the observed pure component-A spectrum. The light curve suggests a contribution of the secondary to the total light of only 6%. Hence, a large range of K_2 must be explored in the spectral disentangling. A further complication in identifying the signal of the secondary is posed by the line profile variability in the primary.

Hence, we discuss in subsequent subsections the spectrum of V2107 Cyg A and the character and cause of the variable metal line profiles. Then, we evaluate the need for a non-circular orbit. Finally, the orbit and the fundamental parameters of the stars are presented.

6.1. The Spectrum of V2107 Cyg A

The spectrum of the hotter component (A) is observed directly near phase 0.5. Comparison with pure rotation profiles (Gray 1992, $\epsilon = 0.6$) for 10 sufficiently unblended metal lines between 4260 and 5740 Å, mainly due to Si III and O II, suggests an apparent rotation velocity of $v \sin i = 84 \pm 4$ km s^{-1}. This value should be interpreted as an upper limit to $v \sin i$ as other velocity fields (macroturbulence, pulsations, etc.) were not considered. A comparison of hydrogen and helium lines with model calculations (LTE line-blanketed models with depth-dependent non-LTE line formation computations, as described in Vrancken et al. 1997), fixing $\log g = 3.6$ cgs as derived from the analysis of the binary, suggests $T_{\rm eff} = 22500 \pm 1500$ K. The uncertainty takes into account that better models are required as lines or line cores formed in higher photospheric layers are inadequately represented (Figure 4). Such detailed analysis is out of the scope of this paper.

Most metal lines show asymmetric line cores. The high-resolution spectra observed at three different epochs in primary eclipse (Figure 5) confirm that V2107 Cyg A is an intrinsic spectrum variable. Since these spectra were taken at essentially the same orbital phase, the origin of the variability is not due to the binary character. With local changes in line depth of up to 4%, the origin must be in the primary component rather than in the secondary which contributes only 6% to the total flux.

Temperature and gravity place V2107 Cyg A in the β Cephei instability strip. The observed type of line profile variations suggests strongly that it is a non-radial pulsator. The photometry supports this viewpoint: the residuals of the orbital light curve show evidence for short-term light variability (Figure 6). In order to enhance the sensitivity for low-amplitude variations, the check was performed on the highest-quality data, with estimated rms uncertainties of 0.005 to 0.008 mag. The selected data set contains 2269 measurements obtained in 15 nights in a time interval of 2 yr, with nightly series covering 2.2 to 6.7 hr. Data in ingress and egress of eclipses were avoided.

The photometric data are suggestive of short-term light variability, either multi-periodic or irregular. A period search did not single out any dominant frequency, although several

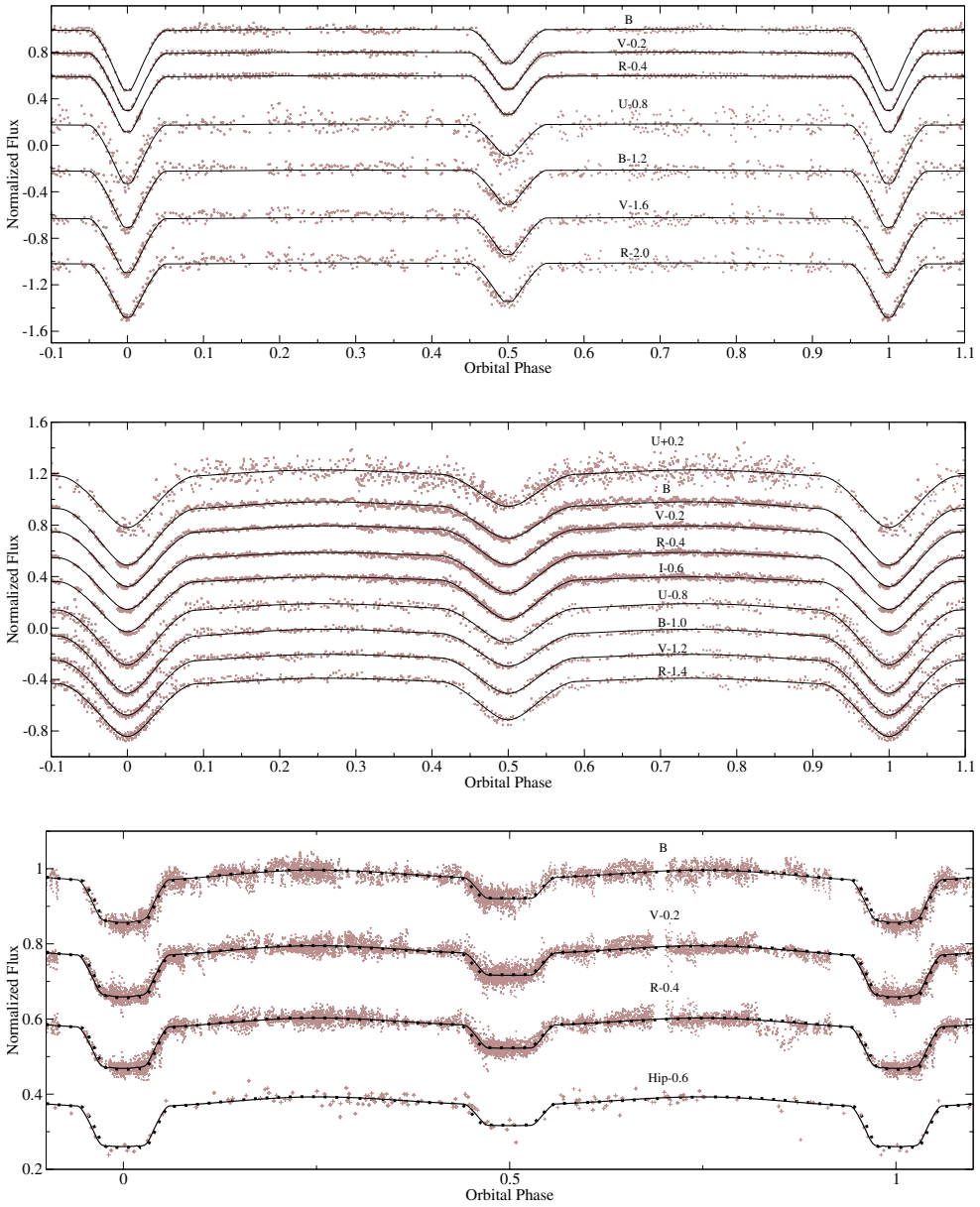

Figure 7. Best fitting LC models (solid lines) for V443 Cyg (top), V456 Cyg (middle), and V2107 Cyg (bottom). For V443 Cyg and V456 Cyg, LC data belonging to the present study and Zakirov & Eshankulova (2005, 2006) are shown with crosses and plus signs, respectively. Eccentric orbit solution for V2107 Cyg is shown with black dots.

(A color version and supplemental data of this figure are available in the online journal.)

peaks (many of them aliases of each other) are above the noise level. Test computations with artificial data and combinations of two frequencies with peaks in the observed power diagram indicate that the noise level and the observed time windows may be insufficient to retrieve the true frequencies uniquely. Nevertheless, the observed light and spectrum variability should encourage larger-scale observational efforts.

6.2. Circular Orbit?

M57 determined the spectroscopic orbit from RV measurements on 16 plates obtained between 1955 July 27 and November 23. Depending on the plate, four to six line positions were measured (He I λ4009.27, λ4120.81, λ4026.19, λ4387.93 and $H\gamma$ and $H\delta$). He notes that only He I λ4009.27 and λ4387.93 are of good quality to measure RVs. Table 3 compares his orbit solution to others derived from the same data and discussed here. All these solutions used $P 4^{\rm d}.2876$ as in M57, but it was checked that updating the orbital period to the value we derived ($4^{\rm d}.2846$) has a negligible effect.

Computing the least-squares eccentric and circular orbits, we confirm the low probability that the orbit is circular ($p = 0.011$) and the LS71 orbital parameters, except their deviating value for the time of periastron passage. The uncertainties mentioned in our solution are computed with the formalism developed in LS71. In view of the evidence for non-radial pulsations that would influence the line position measurements in a non-random way, we also used the jackknife method to estimate bias in the orbital parameters and uncertainties. The bias does not exceed the 1σ level, but, more importantly, the jackknife method suggests larger uncertainties, by a factor of about two, for K and e. Adopting these uncertainties suggests that we should not reject a circular orbit (if we use the LS71 criterion $p > 0.05$).

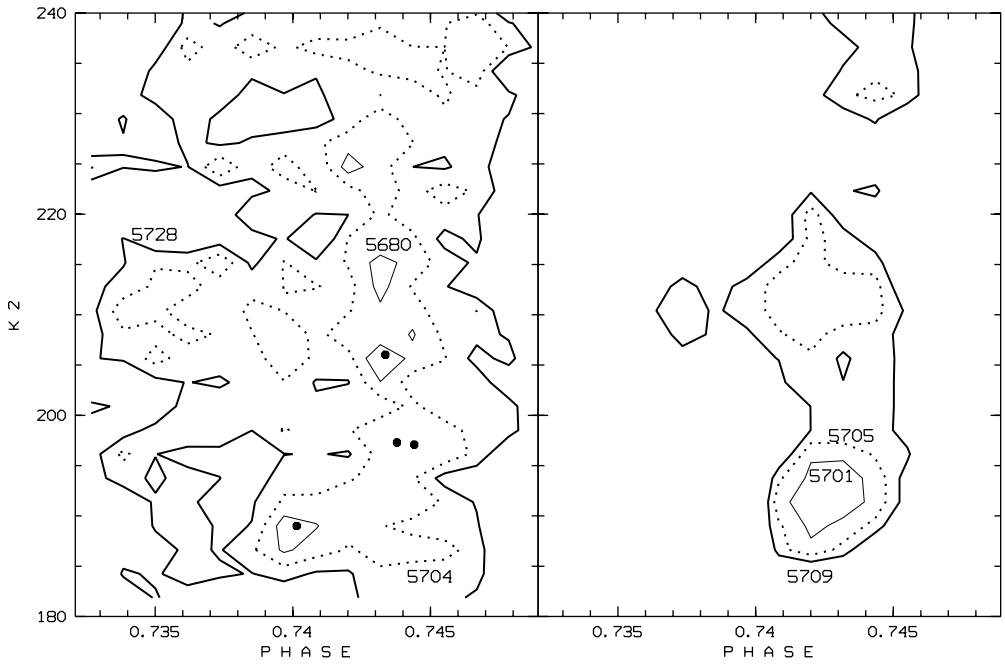

Figure 8. χ^2 map for the H_α region of V2107 Cyg, as seen in the plane (ϕ, K_2), without (left panel) and with (right panel) median filtering to disregard very narrow χ^2 structure. See the explanation in Section 6.2.

Hence, the M57 data may not be sufficient to reject a circular orbit. Using our set of spectroscopic data does not lead to a stronger conclusion.

However, the light curve provides a completely new piece of evidence. Fitting a circular orbit permits ingress and egress of the secondary eclipse systematic residuals that can be removed for a phase separation between the eclipses that is slightly different from half a period, in the sense that the secondary eclipses seen in the *BVR* data occur slightly earlier than half a period after primary eclipse, requiring $e \cos \omega \geqslant 0.015$. Note that the Hipparcos data indicate an opposite effect, if any. However, these data are less straightforward to interpret, both because the eclipses are sparsely covered (from observations in different orbital cycles), and because a significant part of the data in eclipse tends to have larger than average uncertainty estimates in the *Hipparcos* catalog. Taken at face value, a varying time separation between the eclipses might indicate motion of the line of apsides.

Therefore, we searched for solutions that would represent our photometric data as well as the *Hipparcos* ones and the Mercier spectroscopy. The search was made for $0.015 \leqslant e \leqslant 0.07$ taking into account that ω may change with time. Toward larger eccentricities in this interval, the ω value at the time of the recent photometry is nearer to (compared with the M57 epoch) but larger than 90°.

However, we were unable to constrain the eccentricity in this way, as the *Hipparcos* photometry requires an ω value somewhat below 90°, but not so much that almost one full apsidal motion period would have elapsed from M57 to the present time. Higher-precision data are needed to pinpoint the small eccentricity. From the available data, we conclude $e = 0.045 \pm 0.03$. In order to show the need for a non-circular orbit, Figure 7, bottom panel, shows the solution for $e = 0.045$ and $\omega = 102$ deg, as well as for a circular orbit.

Using the H_α region of our spectroscopy, we do not find support for combinations (e, ω) as derived from photometry for $e \geqslant 0.03$, in the sense that such combinations do not lead to solutions with lower chi-square than with a circular orbit. However, in view of the restricted number of spectra and their phase distribution, we prefer not to use this argument to firmly exclude slightly higher eccentricities. Fortunately, K_1 depends on the assumed value e only at the ± 1 km s^{-1} level. The value of K_1 is consistent with RV measurements obtained directly from specific lines (but this classical method leads to larger uncertainty in K_1).

The dependency of K_2 on e is negligible in view of the much larger uncertainty associated with the fact that the signature of the Doppler movement of the faint secondary component is detected only marginally. The signal-to-noise ratio of the *ces* spectroscopy is insufficient to reconstruct any specific feature in the spectrum of the secondary. Only the integrated Doppler signal is detected. In view of the marginal detection, an effort was made to map the multi-dimensional chi-square space in the neighborhood of the deepest minima, for a circular orbit (Figure 8). Test computations for slightly eccentric orbits shows that details of the geometry in chi-square space change with e, but not the global structure.

The detailed gridding reveals the existence of various chi-square minima similar in depth for $185 \leqslant K_2 \leqslant 230$ km s^{-1}, while K_1 and the phase of maximum velocity are well-determined. We constructed the grid up to far outside of this K_2 range, for $K_2 > K_1$, but found no similar minima outside the range quoted above. The most prominent minima are suspiciously narrow, in view of the width of the core of the H_α line, and possibly linked to structure in the noise or in the spectra (telluric lines, pulsation?). Therefore, the right-hand side panel of Figure 8 presents a smoothed version of the chi-square space. The uncertainty quoted for the final spectroscopic orbit (Table 4) and the fundamental parameters of the components (Table 6) take into account the location of the multiple minima, rather than arbitrarily selecting one of the narrow minima.

7. DISCUSSION

Table 6 lists the characteristics of the components and their orbits, as derived from the combined spectroscopic photometric analysis. The proper motions were taken from Roeser et al. (2010), while the distances and systemic velocities of the systems were derived in this study. The space velocity components of the systems were calculated using the algorithm of Johnson & Soderblom (1987) and corrected for the local standard of rest ($U, V, W = 8.50, 13.38, 6.49$) km s^{-1} (Coşkunoğlu et al., 2011). The total space velocities of V2107 Cyg, V443 Cyg, and V456 Cyg are 63, 72, and 14 km s^{-1}, respectively. Applying the N-body code of Dinescu et al. (1999) shows that the three systems move in the Galaxy in moderately eccentric (Galactic) orbits ($e = 0.17, 0.18, 0.07$ for V2107 Cyg, V443 Cyg, and V456 Cyg, respectively). These eccentricities show that the three systems belong to the thin-disk population. However, V2107 Cyg is at a distance of 1.5 ± 0.5 kpc to us, while V443 Cyg (at 0.6 ± 0.2 kpc) and V456 Cyg (at 0.50 ± 0.03 kpc) are much nearer to us.[12] The Mel'nik & Efremov (1995) distance estimate of Cyg OB1 (1.4 kpc) and the Tetzlaff et al. (2010) space velocity components ($U, V, W = 45(2), -27(2), -7(2)$ km s^{-1}) are compatible with V2107 Cyg, which we consider a strong candidate member of this stellar group. In the next subsection we briefly discuss the implications for the star formation history of Cyg OB1.

7.1. V2107 Cyg and the Age of Cyg OB1

The primary component is obviously near the end of the main sequence, while the secondary is near the zero-age main sequence. The fundamental stellar parameters of the secondary suggest a spectral type of B5 V. In view of the light contribution of about 6% to the total light, the core of the diluted hydrogen lines would be 3% deep in the observed spectra and the strongest metal lines, Mg II λ4481 would be 1% deep in the case of rotation synchronized with the orbit. In order to detect these lines with confidence one requires on the order of 15 spectra with S/N of 100. Figure 9 shows the location of the components in the $\log T_{\rm eff} - \log L$ plane, and isochrones calculated using the Web interface.[13] A solar mixture was assumed, i.e., $Z = 0.017$, $Y = 0.26$. Despite the present uncertainties, the age of the system can be constrained to 20 ± 5 Myr due to the favorable position of the primary component. The age estimate of 7.5 Myr for the group as a whole (Mel'nik & Efremov 1995) suggests that star formation may have been ongoing for at least 10^7 yr. Hence, in Cyg OB1 as well as in Cyg OB2 (Comeron & Pasquali 2012), there is evidence in favor of sustained star formation for well over 10 Myr.

This study identifies V2107 Cyg as an extremely interesting binary star with the potential to constrain the duration of the star formation process in the Cyg OB1 association with precision. More extensive high-resolution spectroscopy, as already obtained at the mid-eclipses, is required to constrain K_2 precisely (and thus the mass of the primary). Moreover, with the secondary component of V2107 Cyg occulted for 6 consecutive hours, the intrinsic line profile variations of the primary component can be studied even without the (weak) contamination and dilution by the secondary star. It has been noted, in secondary eclipse, that many metal lines show a peculiar line core with a similar asymmetry, as illustrated for the Si III triplet in Figure 5. Spectroscopic monitoring should confirm that this is due to non-radial pulsations.

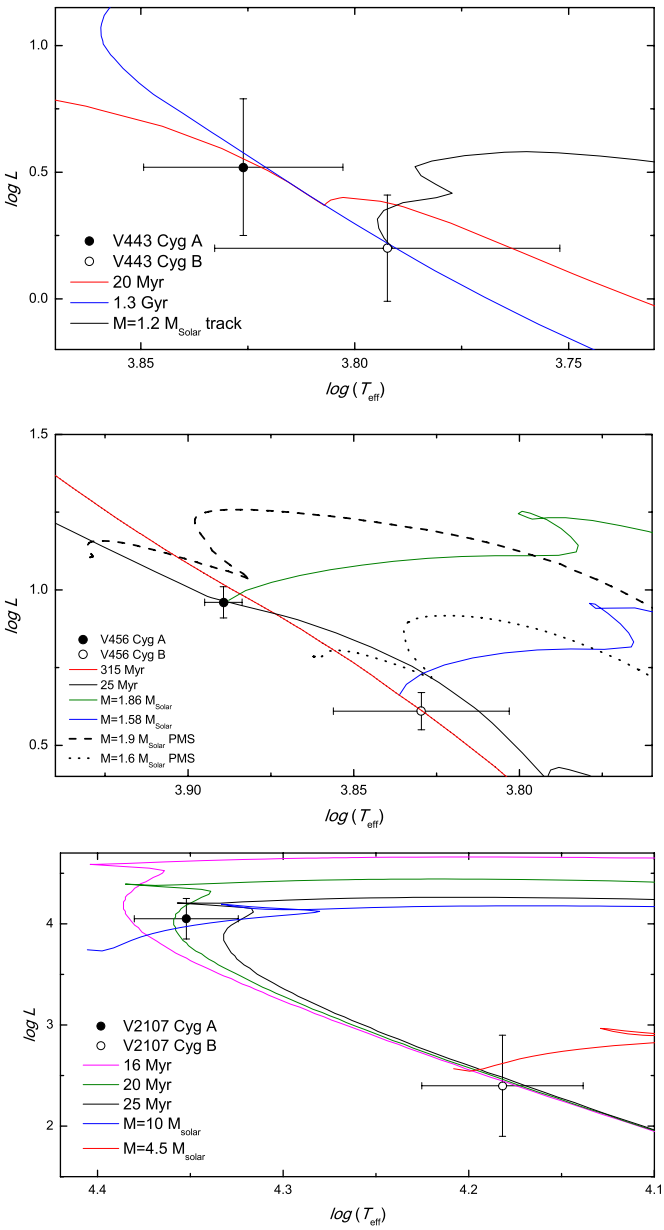

Figure 9. Locations of program stars in the $\log L - \log T_{\rm eff}$ plane together with evolutionary tracks and isochrone curves. Tracks and isochrones for V456 Cyg are calculated for $Z = 0.035$ (full line) and $Z = 0.020$ (dashed; PMS), respectively.

(A color version of this figure is available in the online journal.)

This work is fully supported by the Scientific and Technological Research Council (TÜBİTAK) of Turkey under project code 109T449. The spectroscopic observations are granted by the TÜBİTAK National Observatory with project code 10BRTT150-30-0. The photometric observations are granted by Ulupinar Observatory of Çanakkale Onsekiz Mart University. Part of the spectroscopic observations of V2107 Cyg is based on observations obtained with the HERMES spectrograph, which is supported by the Fund for Scientific Research of Flanders (FWO), Belgium; the Research Council of K.U. Leuven, Belgium; the Fonds National Recherches Scientific (FNRS), Belgium; the Royal Observatory of Belgium; the Observatoire

[12] Bolometric corrections from Straižys & Kuriliene 1981, and $M_{V,\odot} = 4.75$ mag were used.

[13] http://stev.oapd.inaf.it/YZVAR/cgi-bin/form

de Genève, Switzerland; and the Thringer Landessternwarte Tautenburg, Germany. We thank the observers Ben Devries, Yves Frémat, Marie Hrudkova, and Peter Papics. This research made use of SIMBAD and ALADIN. We made use of data from the UVES Paranal Observatory project (ESO DDT Program ID 266.D-5655).

REFERENCES

Bertelli, G., Nasi, E., Girardi, L., & Marigo, P. 2009, A&A, 508, 355
Bikmaev, I., Sakhibullin, N., Musaev, F., & Aslan, Z. 2005, http://www.tug.tubitak.gov.tr
Bissell, A. F., & Ferguson, R. A. 1975, Statistician, 24, 79
Blaha, C., & Humphreys, R. 1989, AJ, 98, 1598
Boeche, C., Munari, U., Tomasella, L., & Barbon, R. 2004, A&A, 415, 145
Cenarro, A. J., Peletier, R. F., Sanchez-Blazquez, P., et al. 2007, MNRAS, 374, 664
Comeron, F., & Pasquali, A. 2012, A&A, 543, A101
Coşkunoğlu, B., Ak, S., Bilir, S., & Karaali, S. 2011, MNRAS, 412, 1237
Cunha, K., Smith, V. V., Boesgaard, A. M., & Lambert, D. L. 2000, ApJ, 530, 939
Dinescu, D. I., Girard, T. M., & van Altena, W. F. 1999, AJ, 117, 1792
Edvardsson, B., Andersen, J., Gustafsson, B., et al. 1993, A&A, 275, 101
ESA 1997, in The Hipparcos and Tycho Catalogues (ESA SP-1200; Noordwijk, ESA)
Gratton, R. G., Carretta, E., & Castelli, F. 1996, A&A, 314, 191
Gray, D. F. 1992, The Observation and Analysis of Stellar Photospheres (2nd ed.; Cambridge: Cambridge Univ. Press)
Gray, R. O. 1988, AJ, 95, 220
Gray, R. O., Corbally, C. F., Garrison, R. F., et al. 2006, A&AS, 209, 8902
Hadrava, P. 1995, A&AS, 114, 393
Hoffman, D. I., Harrison, T. E., Coughlin, J. L., et al. 2008, AJ, 136, 1067
Ilijić, S. 2003, Master thesis, Univ. Zagreb
Johnson, D. R. H., & Soderblom, D. R. 1987, AJ, 93, 864
Kiminki, D. C., & Kobulnicky, H. A. 2012, ApJ, 751, 4
Kobulnicky, H. A., Smullen, R. A., Kiminki, D. C., et al. 2012, ApJ, 756, 50
Kurucz, R. L. 1993, in ASP Conf. Ser. 44, Peculiar versus Normal Phenomena in A-type and Related Stars, ed. M. M. Dworetsky, F. Castelli, & R. Faraggiana (San Francisco, CA: ASP), 87
Lucy, L. B. 1967, ZA, 65, 89
Lucy, L. B., & Sweeney, M. A. 1971, AJ, 76, 544
Mahy, L., Rauw, G., De Becker, M., Eenens, P., & Flores, C. A. 2013, A&A, 550, 27
Mel'nik, A. M., & Efremov, Yu. N. 1995, AstL, 21, 10M
Mercier, J. P. 1957, JO, 40, 12
Morgan, W. W., Code, A. D., & Whitford, A. E. 1955, ApJS, 2, 41
Nelson, R. H. 2011, IBVS, 5994
Prša, A., & Zwitter, T. 2005, ApJ, 628, 426
Raskin, G., van Winckel, H., Hensberge, H., et al. 2011, A&A, 526, 69
Reipurth, B., & Schneider, N. 2008, in Handbook of Star Forming Regions, Volume I: The Northern Sky, ed. B. Reipurth (ASP Monograph Publications, Vol. 4; San Francisco, CA: ASP), 36
Roeser, S., Demleitner, M., & Schilbach, E. 2010, AJ, 139, 2440
Roman, N. G. 1951, ApJ, 114, 492
Rucinski, S. M. 1973, AcA, 23, 79
Straižys, V., & Kuriliene, G. 1981, Ap&SS, 80, 353
Tetzlaff, N., Neuhäuser, R., Hohle, M. M., & Maciejewski, G. 2010, MNRAS, 402, 2369
van Hamme, W. 1993, AJ, 106, 2096
Vrancken, M., Hensberge, H., David, M., & Verschueren, W. 1997, A&A, 320, 878
Walborn, N. R. 1971, ApJS, 23, 257
Wilson, R. E. 1990, ApJ, 356, 613
Wilson, R. E., & Devinney, E. J. 1971, ApJ, 166, 605
Wolk, S. J., Rice, T. S., & Aspin, C. A. 2013, AJ, 145, 113
Wozniak, P. R., Vestrand, W. T., Akerlof, C. W., et al. 2004, AJ, 127, 2436
Zakirov, M. M. 1999, AstL, 25, 229
Zakirov, M. M., & Eshankulova, M. U. 2005, KFNT, 21, 441
Zakirov, M. M., & Eshankulova, M. U. 2006, KFNT, 22, 363